

# Large Spin Hall Magnetoresistance in Antiferromagnetic $\alpha$ -Fe<sub>2</sub>O<sub>3</sub>/Pt Heterostructures

Johanna Fischer<sup>1,2,†</sup>, Matthias Althammer<sup>1,2</sup>, Nynke Vlietstra,<sup>1,2</sup> Hans Huebl<sup>1,2</sup>, Sebastian T.B. Goennenwein<sup>3,4</sup>, Rudolf Gross<sup>1,2,5</sup>, Stephan Geprägs<sup>1</sup>, and Matthias Opel<sup>1,\*</sup>

<sup>1</sup>Walther-Meissner-Institut, Bayerische Akademie der Wissenschaften, 85748 Garching, Germany

<sup>2</sup>Physik-Department, Technische Universität München, 85748 Garching, Germany

<sup>3</sup>Institut für Festkörper- und Materialphysik, Technische Universität Dresden, 01062 Dresden, Germany

<sup>4</sup>Center for Transport and Devices of Emergent Materials, Technische Universität Dresden, 01062 Dresden, Germany

<sup>5</sup>Munich Center for Quantum Science and Technology (MCQST), 80799 Munich, Germany



(Received 29 July 2019; revised manuscript received 14 October 2019; published 13 January 2020)

We investigate the spin Hall magnetoresistance (SMR) at room temperature in thin-film heterostructures of antiferromagnetic insulating (0001)-oriented  $\alpha$ -Fe<sub>2</sub>O<sub>3</sub> (hematite) and Pt. We measure their longitudinal and transverse resistivities while rotating an applied magnetic field of up to 17 T in three orthogonal planes. For out-of-plane magnetotransport measurements, we find indications for a multidomain antiferromagnetic configuration whenever the field is aligned along the film normal. For in-plane field rotations, we clearly observe a sinusoidal resistivity oscillation characteristic for the SMR due to a coherent rotation of the Néel vector. The maximum SMR amplitude of 0.25% is, surprisingly, twice as high as for prototypical ferrimagnetic Y<sub>3</sub>Fe<sub>5</sub>O<sub>12</sub>/Pt heterostructures. The SMR effect saturates at much smaller magnetic fields than in comparable antiferromagnets, making the  $\alpha$ -Fe<sub>2</sub>O<sub>3</sub>/Pt system particularly interesting for room-temperature antiferromagnetic spintronic applications.

DOI: 10.1103/PhysRevApplied.13.014019

## I. INTRODUCTION

Despite lacking a net macroscopic magnetization, antiferromagnetic (AF) materials have moved into the focus of spintronics research [1–4]. Although Néel [5] stated about 50 years ago that antiferromagnets “are extremely interesting from the theoretical viewpoint, but do not seem to have any applications,” this class of materials confers two important advantages compared to ferromagnets: (i) they enable a better scalability and a higher robustness against magnetic field perturbations [1–3]; and (ii) they offer orders-of-magnitude-faster dynamics and thus switching times [6,7]. Accordingly, AF spintronics has emerged rapidly and has led to important developments ranging from random-access-memory schemes [8,9] and the discovery of the spin colossal magnetoresistance [10] in magnetoelectric antiferromagnets via synthetic antiferromagnetic spintronic devices [11,12] to the demonstration of long-range magnon spin transport in intrinsic antiferromagnets [13]. From an application perspective, both the

switching of the AF state as well as the reading out of the AF sublattice magnetization orientations are important challenges. It is evident that the vanishing net moment and the very small stray fields in AF materials call for new magnetization control and readout strategies.

Spin currents [14] have been shown to interact with individual magnetic sublattices via spin transfer torques also in antiferromagnets [15–18]. A particular manifestation of spin-torque physics is the dependence of the resistivity of a metallic thin film with large spin-orbit coupling on the direction of the magnetization in an adjacent material with long-range magnetic order, denoted as the spin Hall magnetoresistance (SMR) effect [19–22]. Following earlier results in all-metallic systems [23], the SMR was first established in oxide spintronics [24] for insulating collinear ferrimagnetic Y<sub>3</sub>Fe<sub>5</sub>O<sub>12</sub>/Pt bilayers [19–21]. Upon rotating the magnetization in the magnet-metal interface plane, the SMR appears as a sinusoidal oscillation of the Pt resistivity, characterized by a specific amplitude and a phase. In compensated ferrimagnetic YGd<sub>2</sub>Fe<sub>4</sub>InO<sub>12</sub>/Pt heterostructures, the pronounced temperature dependence of the SMR phase demonstrates the sensitivity of the effect to the individual canted Fe<sup>3+</sup> sublattice magnetizations [25]. Recently, the SMR effect has also been identified in AF heterostructures. In spite of their zero net

\* matthias.opel@wmi.badw.de

† Present address: Unité Mixte de Physique, CNRS, Thales, Université Paris-Sud, Université Paris-Saclay, 91767 Palaiseau, France.

magnetization, the AF ordered magnetic sublattices contribute individually, resulting in a nonzero SMR. As the sublattice magnetizations are orthogonal to the applied magnetic field, a phase shift of  $90^\circ$  has been reported for the SMR in NiO/Pt [26–28] and Cr<sub>2</sub>O<sub>3</sub>/Ta [29] as well as all-metallic PtMn/Pt [30] and PtMn/W [30] compared to that in the prototypical ferrimagnetic Y<sub>3</sub>Fe<sub>5</sub>O<sub>12</sub>/Pt heterostructures. The SMR amplitude is still a matter of debate, since various extrinsic as well as intrinsic parameters play a crucial role [17,31,32] and some authors report a nonzero amplitude even above the respective magnetic ordering temperatures [33,34].

In this paper, we substantially complement the SMR data available for AF insulators by investigating  $\alpha$ -Fe<sub>2</sub>O<sub>3</sub>/Pt. We find a surprisingly large SMR amplitude of 0.25%, much higher than in AF NiO/Pt [27] and twice as large as in Y<sub>3</sub>Fe<sub>5</sub>O<sub>12</sub>/Pt [21]. This finding supports the picture that both AF sublattices contribute to the SMR at the interface, regardless of the material's net magnetization. The large SMR amplitude together with a moderate saturation field of approximately 3 T establishes  $\alpha$ -Fe<sub>2</sub>O<sub>3</sub>/Pt as a viable future SMR source and paves the way toward room-temperature antiferromagnetic spintronic applications.

## II. THIN-FILM DEPOSITION AND STRUCTURAL CHARACTERIZATION

The electrical insulator  $\alpha$ -Fe<sub>2</sub>O<sub>3</sub> (hematite) crystallizes in a rhombohedral structure and can be described in the hexagonal system with the lattice constants  $a = 0.5032$  nm and  $c = 1.3748$  nm [35]. In bulk, it exhibits a Néel temperature of  $T_N = 953$  K and undergoes a spin reorientation (“Morin” transition) at  $T_M \approx 263$  K [36]. For  $T_M < T < T_N$  and in the absence of an external magnetic field, the  $S = 5/2$  spins of the Fe<sup>3+</sup> ions are ordered ferromagnetically in the (0001) planes. Along the crystallographic [0001] direction, these easy planes form a “+ − − +” sequence, resulting in a net AF order [37]. A finite anisotropic spin-spin (“Dzyaloshinskii-Moriya”) interaction [38,39] leads to a small canting of the two AF sublattice magnetizations  $\mathbf{M}_1$  and  $\mathbf{M}_2$  with a canting angle of  $0.13^\circ \pm 0.01^\circ$  [40]. This results in a small net magnetization  $\mathbf{M} = \mathbf{M}_1 + \mathbf{M}_2$  in the (0001) plane. Similar to the situation in NiO [27],  $\alpha$ -Fe<sub>2</sub>O<sub>3</sub> displays three AF domains rotated by  $120^\circ$  with respect to each other [41,42] and a domain population dependent on the direction and magnitude of the external magnetic field [42]. The monodomainization field  $\mu_0 H_{MD}$  is reported to be above 600 mT [42].

Since thin films are key for applications, here we study  $\alpha$ -Fe<sub>2</sub>O<sub>3</sub>/Pt bilayer heterostructures, fabricated on single-crystalline (0001)-oriented Al<sub>2</sub>O<sub>3</sub> substrates. Using our pulsed laser deposition setup described in Ref. [43], we

first deposit epitaxial  $\alpha$ -Fe<sub>2</sub>O<sub>3</sub> thin films from a stoichiometric target with a laser fluence and a repetition rate of  $2.5$  J/cm<sup>2</sup> and 2 Hz, respectively, at a substrate temperature of 320 °C in an oxygen atmosphere of 25 μbar. Without breaking the vacuum, the films are then covered *in situ* by thin layers of Pt via electron-beam evaporation. High-resolution x-ray diffractometry (HR-XRD) measurements reveal a high structural quality of the  $\alpha$ -Fe<sub>2</sub>O<sub>3</sub>/Pt heterostructures. The  $2\theta-\omega$  scan [Fig. 1(a)] shows only reflections from the epitaxial  $\alpha$ -Fe<sub>2</sub>O<sub>3</sub> thin

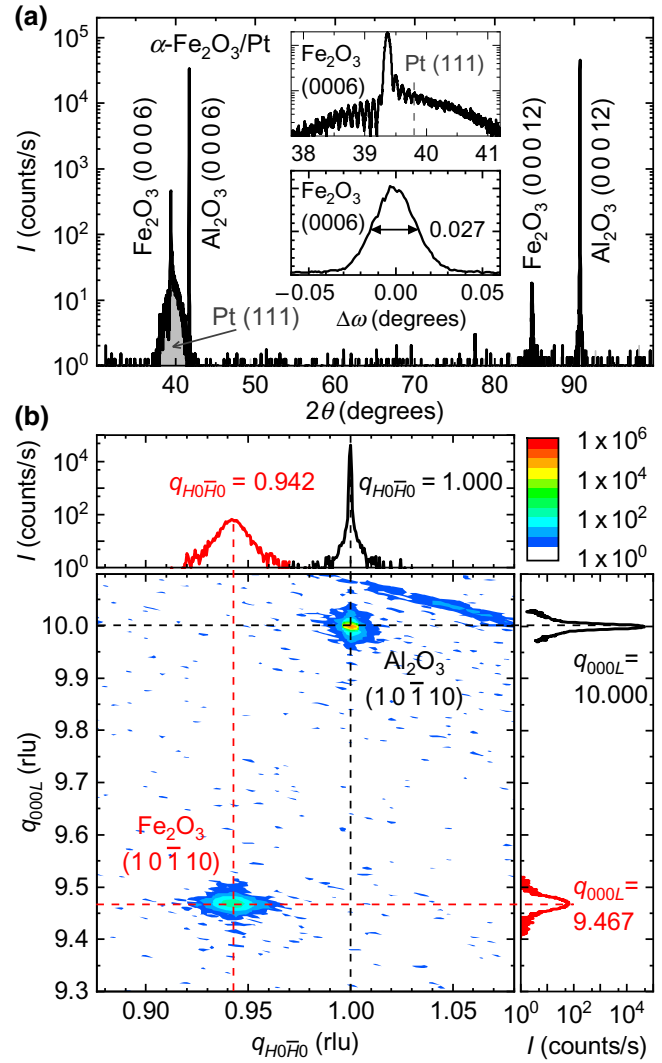


FIG. 1. The structural properties of the investigated  $\alpha$ -Fe<sub>2</sub>O<sub>3</sub>/Pt heterostructure fabricated on a (0001)-oriented Al<sub>2</sub>O<sub>3</sub> substrate. (a)  $2\theta-\omega$  scan along the [0001] direction of Al<sub>2</sub>O<sub>3</sub>. The upper inset shows the scan on an enlarged scale together with the expected position of the Pt(111) reflection (vertical dashed line). The lower inset displays the rocking curve around the  $\alpha$ -Fe<sub>2</sub>O<sub>3</sub>(0006) reflection with a full width at half maximum of only 0.027°. (b) Reciprocal space mapping around the (10̄110) reflections. The reciprocal lattice unit (rlu) is related to the Al<sub>2</sub>O<sub>3</sub> substrate reflection.

film, the Pt layer, and the Al<sub>2</sub>O<sub>3</sub> substrate. No secondary crystalline phases are detected. A broad feature below the  $\alpha$ -Fe<sub>2</sub>O<sub>3</sub>(0006) reflection (gray shaded area) can be assigned to Pt(111) expected at 39.8° and points to a textured nature of the Pt top electrode. On an enlarged scale [the upper inset in Fig. 1(a)], satellites due to Laue oscillations are detected around the  $\alpha$ -Fe<sub>2</sub>O<sub>3</sub>(0006) reflection, evidencing a coherent growth with low interface roughness of the  $\alpha$ -Fe<sub>2</sub>O<sub>3</sub> thin film. The asymmetry on both sides of the  $\alpha$ -Fe<sub>2</sub>O<sub>3</sub>(0006) reflection is caused by interference with the broad Pt(111) reflection. Furthermore,  $\alpha$ -Fe<sub>2</sub>O<sub>3</sub> shows a low mosaic spread, as demonstrated by the full width at half maximum of the rocking curve around the  $\alpha$ -Fe<sub>2</sub>O<sub>3</sub>(0006) reflection of only 0.027° [the lower inset in Fig. 1(a)]. The in-plane orientation and strain state are investigated by reciprocal space mappings around the (10̄10) reflections [Fig. 1(b)]. They reveal the epitaxial relations [0001] $\alpha$ -Fe<sub>2</sub>O<sub>3</sub>||[0001]Al<sub>2</sub>O<sub>3</sub> and [10̄10] $\alpha$ -Fe<sub>2</sub>O<sub>3</sub>||[1010]Al<sub>2</sub>O<sub>3</sub>. We derive lattice constants of  $a = 0.505$  nm and  $c = 1.372$  nm, very close to the respective bulk values, indicating a nearly fully relaxed strain state for our  $\alpha$ -Fe<sub>2</sub>O<sub>3</sub> films. Furthermore, a low interface and a low surface roughness of 0.90 nm and 0.76 nm (rms values), respectively, are confirmed by x-ray reflectivity [44]. We note that up to now, no clear recipe has been established to prepare a monophase termination of  $\alpha$ -Fe<sub>2</sub>O<sub>3</sub>(0001) [45]. Density-functional-theory- (DFT) based calculations suggest that a Fe termination containing half of the interplane Fe is stable at low oxygen pressures [46]. Together with an interface roughness of our sample exceeding the interlayer distance of 0.23 nm, this suggests that Fe<sup>3+</sup> spins of both magnetic sublattices (i.e., with opposite directions) are present at the Pt/ $\alpha$ -Fe<sub>2</sub>O<sub>3</sub> interface. In summary, our  $\alpha$ -Fe<sub>2</sub>O<sub>3</sub>/Pt bilayer is of the same high structural quality as the prototypical ferrimagnetic Y<sub>3</sub>Fe<sub>5</sub>O<sub>12</sub>/Pt heterostructures reported earlier [21].

### III. ANGLE DEPENDENCE OF THE SPIN HALL MAGNETORESISTANCE

In the following, we discuss an  $\alpha$ -Fe<sub>2</sub>O<sub>3</sub>/Pt bilayer sample with thicknesses of  $t_{\text{Fe}_2\text{O}_3} = 91.4$  nm and  $t_{\text{Pt}} = 3.0$  nm. For transport measurements, a Hall bar-shaped mesa structure with a width of  $w = 81 \mu\text{m}$  and a longitudinal contact separation (length) of  $l = 609 \mu\text{m}$  is patterned into the bilayer via photolithography and Ar ion milling (Fig. 2). For a dc current of  $\pm 100 \mu\text{A}$  applied in the [1010] direction, the longitudinal ( $\rho_{\text{long}}$ ) and the transverse ( $\rho_{\text{trans}}$ ) resistivities are measured in a standard four-probe configuration. A current-reversal method is applied to eliminate thermal effects [25]. We restrict our investigation to room temperature, where the (0001) plane is a magnetic easy plane. We perform angle-dependent magnetoresistance (ADMR) measurements by rotating an external magnetic field of constant magnitude  $H$  in three different

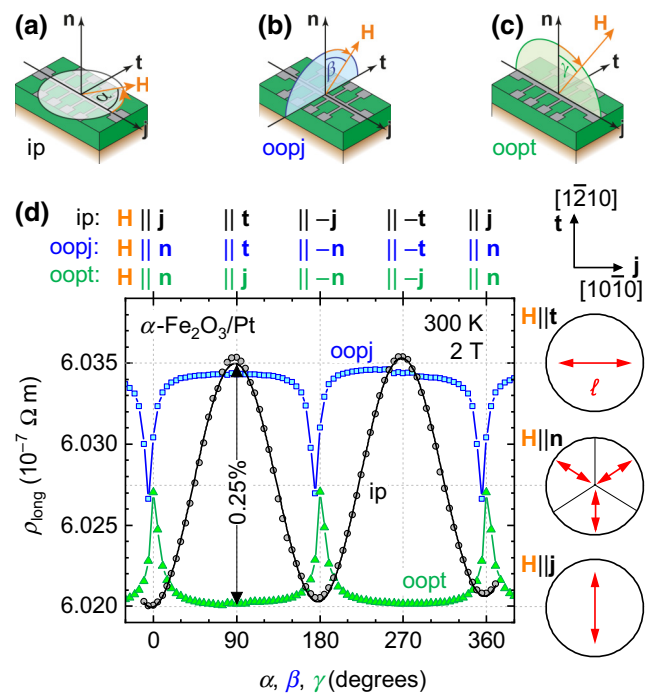


FIG. 2. The ADMR of a (0001)-oriented  $\alpha$ -Fe<sub>2</sub>O<sub>3</sub>/Pt heterostructure. The external magnetic field  $\mathbf{H}$  is rotated in three different planes: (a) in the film plane (ip, angle  $\alpha$ ), (b) perpendicular to the current direction  $\mathbf{j}$  (oopj,  $\beta$ ), and (c) perpendicular to the transverse direction  $\mathbf{t}$  (oopt,  $\gamma$ ). The vector  $\mathbf{n}$  denotes the film normal. (d) The longitudinal resistivity  $\rho_{\text{long}}$  is recorded at 300 K and 2 T for all three rotation planes: ip (black circles), oopj (blue squares), and oopt (green triangles). The black line is a fit to the ip data according to Eq. (1), while the blue and green lines are guides to the eye. The SMR amplitude of 0.25% (vertical black double arrow) is significantly larger than in prototypical Y<sub>3</sub>Fe<sub>5</sub>O<sub>12</sub>/Pt structures. At the high (low) resistivity level,  $\alpha$ -Fe<sub>2</sub>O<sub>3</sub> is in a monodomain state with the Néel vector  $\ell$  pointing parallel (perpendicular) to  $\mathbf{j}$  with  $\mathbf{H} \parallel \mathbf{t}$  ( $\mathbf{H} \parallel \mathbf{j}$ ). For  $\mathbf{H} \parallel \mathbf{n}$ , only occurring in oopj and oopt geometry,  $\alpha$ -Fe<sub>2</sub>O<sub>3</sub> exhibits a multidomain state with medium resistivity. The corresponding domain patterns are illustrated to the right, besides the data plots.

orthogonal planes of the (0001)-oriented  $\alpha$ -Fe<sub>2</sub>O<sub>3</sub>, using the same notation as in Ref. [21] and Figs. 2(a)–2(c): (0001) = “ip” (in-plane, angle  $\alpha$ , black); (10̄10) = “oopj” (out-of-plane perpendicular to  $\mathbf{j}$ , angle  $\beta$ , blue); (12̄10) = “oopt” (out-of-plane perpendicular to  $\mathbf{t}$ , angle  $\gamma$ , green).

For ip rotations at  $\mu_0 H = 2$  T,  $\rho_{\text{long}}(\alpha)$  displays the characteristic SMR oscillations with 180° period [black circles in Fig. 2(d)]. The minima and maxima are located at  $\mathbf{H} \parallel \pm \mathbf{j}$  and  $\mathbf{H} \parallel \pm \mathbf{t}$ , respectively, representing the signature of the AF (“negative”) SMR [26–28] with a phase shift of 90° compared to the ferromagnetic (“positive”) SMR in ferrimagnetic Y<sub>3</sub>Fe<sub>5</sub>O<sub>12</sub>/Pt [21,22] or  $\gamma$ -Fe<sub>2</sub>O<sub>3</sub>/Pt [47]. The SMR amplitude is almost saturated at  $\mu_0 H = 2$  T (see below). We can safely assume a monodomain state of the  $\alpha$ -Fe<sub>2</sub>O<sub>3</sub> thin film with the Néel vector  $\ell = (\mathbf{m}_1 - \mathbf{m}_2)/2$

with  $\mathbf{m}_i = \mathbf{M}_i/|\mathbf{M}_i|$  rotating coherently and perpendicular to  $\mathbf{H}$  in the magnetic easy (0001) plane. The data are well described by

$$\rho_{\text{long}} = \rho_0 + \frac{\rho_1}{2}(1 - \cos 2\alpha), \quad (1)$$

$$\rho_{\text{trans}} = -\frac{\rho_3}{2} \sin 2\alpha, \quad (2)$$

[black line in Fig. 2(d)] with  $\rho_0$  approximately equal to the normal resistivity of the Pt layer and  $\rho_1$  and  $\rho_3$  representing the longitudinal and the transverse SMR coefficients, respectively [44], as demonstrated earlier for AF NiO/Pt [27]. However, the SMR amplitude of 0.25% for  $\alpha\text{-Fe}_2\text{O}_3/\text{Pt}$  is more than a factor of 3 higher than for NiO/Pt and, remarkably, even twice as large as for the prototypical ferrimagnetic  $\text{Y}_3\text{Fe}_5\text{O}_{12}/\text{Pt}$  heterostructures with a similar Pt thickness [21]. In fact, it is larger than for any other reported bilayer compound so far. We attribute this to the large density of magnetic  $\text{Fe}^{3+}$  ions in  $\alpha\text{-Fe}_2\text{O}_3$ . With a spin Hall angle of 0.11 and a spin diffusion length of 1.5 nm for Pt [31], we calculate  $G_r = 1.38 \times 10^{15} \Omega^{-1} \text{ m}^{-2}$  for the real part of the spin-mixing interface conductance. Although the situation regarding the magnitude of  $G_r$  is confusing, since the values reported in the literature are obtained from different techniques and are not fully comparable to each other [48], our value is of the order of all-metallic ferromagnetic interfaces [49,50]. It is consistent with that reported by Cheng and coworkers for antiferromagnetic  $\alpha\text{-Fe}_2\text{O}_3/\text{Pt}$  [51] and about one order of magnitude larger than for ferrimagnetic  $\text{Y}_3\text{Fe}_5\text{O}_{12}/\text{Pt}$  heterostructures [21,31].

The ADMR of the out-of-plane rotations is qualitatively different. For oopj rotations of  $\mathbf{H}$ , we observe  $\rho_{\text{long}}$  in the maximum resistive state for a wide range of angles  $\beta$  around  $\mathbf{H} \parallel \pm\mathbf{t}$  [blue squares in Fig. 2(d)], indicating a monodomain state with  $\ell \parallel \pm\mathbf{j}$ . For the oopt geometry, on the other hand,  $\rho_{\text{long}}$  stays in the minimum resistive state for a wide range of angles  $\gamma$  around  $\mathbf{H} \parallel \pm\mathbf{t}$  [green triangles in Fig. 2(d)], again indicating a monodomain state with  $\ell \parallel \pm\mathbf{t}$ . Both observations show that  $\ell$  does not follow  $\mathbf{H}$  for out-of-plane rotations.  $\rho_{\text{long}}$  changes significantly only close to  $\mathbf{H} \parallel \pm\mathbf{n}$ : both the oopj and the oopt curves meet for magnetic fields perpendicular to the sample surface at the midpoint of the two states with extremal resistance. According to the SMR model for a multidomain antiferromagnet [27], we interpret this observation as the “decay” of a monodomain into a three-domain state when  $\mathbf{H}$  points orthogonal to the magnetic easy (0001) plane of  $\alpha\text{-Fe}_2\text{O}_3$ , in agreement with a recent preprint [51].

#### IV. FIELD DEPENDENCE OF THE SPIN HALL MAGNETORESISTANCE

To obtain further insight into the AF domain configurations, we perform ip ADMR measurements of both  $\rho_{\text{long}}$

and  $\rho_{\text{trans}}$  at different magnitudes of the magnetic field from 10 mT to 17 T (Fig. 3). The expected  $(-\cos 2\alpha)$  and  $(-\sin 2\alpha)$  dependencies of  $\rho_{\text{long}}$  and  $\rho_{\text{trans}}$ , respectively, are clearly observed for  $\mu_0 H \geq 300$  mT [Figs. 3(b)–3(e)]. This angular dependence is fully consistent with the model introduced earlier for NiO/Pt [27] and Eqs. (1) and (2) and clearly shows that our  $\alpha\text{-Fe}_2\text{O}_3$  is AF, with the resistivity of Pt being sensitive to  $\ell$ , which rotates coherently in the easy (0001) plane perpendicular to  $\mathbf{H}$ . The data is further fully consistent with recent experiments in Pt on canted ferrimagnets, where the same angular dependence is observed close to the compensation temperature [25], as well as experiments in  $\text{Y}_3\text{Fe}_5\text{O}_{12}/\text{NiO}/\text{Pt}$  [52–55] and NiO/Pt [26–28]. For  $\mu_0 H \lesssim 100$  mT, the applied field is smaller than  $\mu_0 H_{\text{MD}}$ , resulting in hardly detectable SMR oscillations [Fig. 3(a)].

For a detailed analysis of the field dependence of  $\rho_{\text{long}}$  and  $\rho_{\text{trans}}$ , we fit our data analogous to Eqs. (1) and (2) using  $\cos 2\alpha$  and  $\sin 2\alpha$  functions, respectively (solid lines

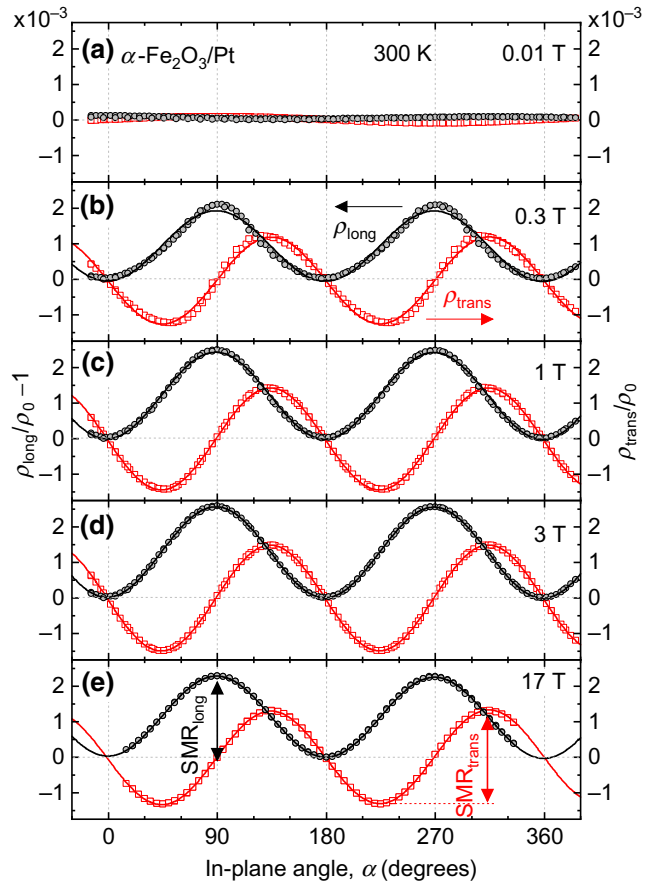


FIG. 3. The in-plane ADMR of a (0001)-oriented  $\alpha\text{-Fe}_2\text{O}_3/\text{Pt}$  heterostructure at 300 K in magnetic fields of (a) 0.01 T, (b) 0.3 T, (c) 1 T, (d) 3 T, and (e) 17 T. The normalized longitudinal ( $\rho_{\text{long}}$ , black circles, left axis) and transverse resistivities ( $\rho_{\text{trans}}$ , red squares, right axis) are plotted as a function of the in-plane magnetic field orientation  $\alpha$ . The lines are fits to the data using  $\cos 2\alpha$  and  $\sin 2\alpha$  functions analogous to Eqs. (1) and (2).

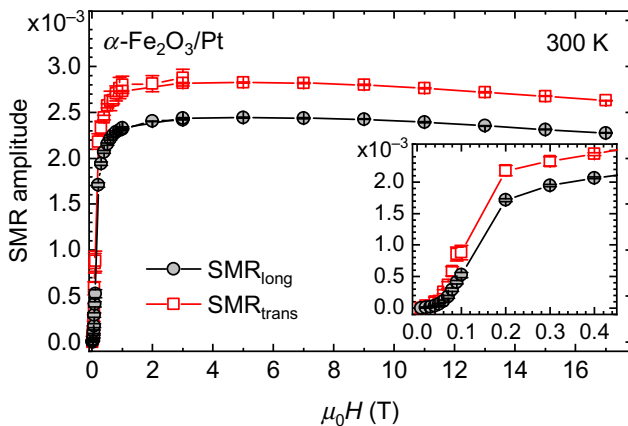


FIG. 4. The SMR amplitudes  $\text{SMR}_{\text{long}}$  (black circles) and  $\text{SMR}_{\text{trans}}$  (red squares) of a (0001)-oriented  $\alpha$ -Fe<sub>2</sub>O<sub>3</sub>/Pt heterostructure derived from ADMR measurements at 300 K in different external magnetic fields  $H$  (cf. Fig. 3).

in Fig. 3), and plot the SMR amplitudes  $\text{SMR}_{\text{long}}$  and  $\text{SMR}_{\text{trans}}$  [double arrows in Fig. 3(e)] as a function of the magnetic field magnitude in Fig. 4. Remarkably,  $\text{SMR}_{\text{trans}}$  exceeds  $\text{SMR}_{\text{long}}$  for fields above 100 mT. This unexpected observation may indicate the presence of large 180° domains in  $\alpha$ -Fe<sub>2</sub>O<sub>3</sub>, exceeding the width of the Hall bar. Thick 180° domain walls, present only along the length of the Hall bar, might then effectively reduce the SMR in the longitudinal voltage but not in the transverse one. We note that such large domains and thick domain walls have been reported for (0001)-oriented bulk material at moderate magnetic fields [40,56,57] but cannot be resolved in (0001)-oriented thin films at room temperature in a zero magnetic field [58].

Furthermore, the field evolution of the SMR amplitude is qualitatively different from the one in AF NiO/Pt [27]. In  $\alpha$ -Fe<sub>2</sub>O<sub>3</sub>/Pt, we find that both  $\text{SMR}_{\text{long}}$  and  $\text{SMR}_{\text{trans}}$  are already saturated around 3 T and then gradually decrease again from 5 T to 17 T. This gradual decrease can be traced back to an increasing canting of the AF sublattices, thus reducing the value of  $\ell$ , and an emerging nonzero net  $\mathbf{M}$  [44]. The fast saturation, on the other hand, points to a lower destressing energy compared to NiO. The field dependence of the SMR amplitude indicates that the 120° domains in our  $\alpha$ -Fe<sub>2</sub>O<sub>3</sub> thin film vanish at approximately 3 T, where the SMR amplitude starts to saturate (Fig. 4). To quantify the destressing effects, we identify 3 T with the monodomainization field  $H_{\text{MD}}$ , since the leftover 180° domains have indistinguishable destressing energy density. With an exchange field of  $\mu_0 H_{\text{ex}} = 900$  T [40,59], we derive a destressing field  $\mu_0 H_{\text{dest}} = \mu_0 H_{\text{MD}}^2 / (4H_{\text{ex}}) \approx 2.5$  mT, smaller than the 46 mT in epitaxial NiO thin films on Al<sub>2</sub>O<sub>3</sub> [27]. This value is reasonable, since the magnetostriction  $\lambda = 4 \times 10^{-6}$  in the basal plane of  $\alpha$ -Fe<sub>2</sub>O<sub>3</sub> at

293 K [60] is smaller than  $\lambda = (9 \pm 3) \times 10^{-5}$  in NiO, by a factor of approximately 20 [61].

## V. CONCLUSION AND OUTLOOK

In summary, we present a detailed investigation of the SMR in antiferromagnetic  $\alpha$ -Fe<sub>2</sub>O<sub>3</sub>/Pt heterostructures at room temperature, studying three orthogonal rotation planes of the magnetic field. We consistently describe the angular dependence of the data in a three-domain model, considering a field-dependent canting of the AF sublattices. Our data support the picture that each magnetic sublattice contributes separately to the SMR. Surprisingly, we find a large SMR amplitude of 0.25%. This value is well in excess of the established values for Y<sub>3</sub>Fe<sub>5</sub>O<sub>12</sub>/Pt or any other Pt-based thin-film heterostructures reported in the literature so far. AF materials are therefore expected to play an important role in SMR-related research and applications. Due to the small destressing field, the SMR amplitude already reaches 0.20% (corresponding to  $\frac{4}{5}$  of its maximum value) at 300 mT, i.e., at much smaller magnetic fields than in comparable AF NiO/Pt heterostructures [27]. This combination of high sensitivity at low magnetic fields and room-temperature operation makes  $\alpha$ -Fe<sub>2</sub>O<sub>3</sub>/Pt a promising material system both for a viable SMR source and future spin-transfer torque-based devices. The large spin-mixing interface conductance of  $1.38 \times 10^{15} \Omega^{-1} \text{m}^{-2}$  makes it further suitable for spin-current-induced magnetization switching or other spin-transfer torque-based applications in the emerging field of antiferromagnetic spintronics.

## ACKNOWLEDGMENTS

We thank T. Brenninger, A. Habel, and K. Helm-Knapp for technical support, as well as O. Gomonay and A. Kamra for fruitful discussions. We gratefully acknowledge the financial support of the German Research Foundation via Germany's Excellence Strategy (Grant No. EXC-2111-390814868). N.V. acknowledges support from a Laura-Bassi stipend of the Technical University of Munich.

- 
- [1] X. Marti *et al.*, Room-temperature antiferromagnetic memory resistor, *Nat. Mater.* **13**, 367 (2014).
  - [2] P. Wadley *et al.*, Electrical switching of an antiferromagnet, *Science* **351**, 587 (2016).
  - [3] T. Jungwirth, X. Marti, P. Wadley, and J. Wunderlich, Antiferromagnetic spintronics, *Nat. Nanotechnol.* **11**, 231 (2016).
  - [4] V. Baltz, A. Manchon, M. Tsoi, T. Moriyama, T. Ono, and Y. Tserkovnyak, Antiferromagnetic spintronics, *Rev. Mod. Phys.* **90**, 015005 (2018).
  - [5] L. Néel, Magnetism and the local molecular field, in: *Nobel Lectures, Physics 1963–1970* (Elsevier Publishing

- Company, Amsterdam, 1972), <https://www.nobelprize.org/prizes/physics/1970/neel/lecture/>
- [6] T. Satoh, R. Iida, T. Higuchi, M. Fiebig, and T. Shimura, Writing and reading of an arbitrary optical polarization state in an antiferromagnet, *Nat. Photonics* **9**, 25 (2014).
- [7] K. Olejník, T. Seifert, Z. Kašpar, V. Novák, P. Wadley, R. P. Campion, M. Baumgartner, P. Gambardella, P. Němec, J. Wunderlich, J. Sinova, P. Kužel, M. Müller, T. Kampfrath, and T. Jungwirth, Terahertz electrical writing speed in an antiferromagnetic memory, *Sci. Adv.* **4**, 3566 (2018).
- [8] T. Kosub, M. Kopte, F. Radu, O. G. Schmidt, and D. Makarov, All-Electric Access to the Magnetic-Field-Invariant Magnetization of Antiferromagnets, *Phys. Rev. Lett.* **115**, 097201 (2015).
- [9] T. Kosub, M. Kopte, R. Hühne, P. Appel, B. Shields, P. Maletinsky, R. Hübner, M. O. Liedke, J. Fassbender, O. G. Schmidt, and D. Makarov, Purely antiferromagnetic magnetoelectric random access memory, *Nat. Commun.* **8**, 13985 (2017).
- [10] Z. Qiu, D. Hou, J. Barker, K. Yamamoto, O. Gomonay, and E. Saitoh, Spin colossal magnetoresistance in an antiferromagnetic insulator, *Nat. Mater.* **17**, 577 (2018).
- [11] J. M. Gomez-Perez, S. Vélez, L. McKenzie-Sell, M. Amado, J. Herrero-Martín, J. López-López, S. Blanco-Canosa, L. E. Hueso, A. Chuvalin, J. W. A. Robinson, and F. Casanova, Synthetic Antiferromagnetic Coupling Between Ultrathin Insulating Garnets, *Phys. Rev. Appl.* **10**, 044046 (2018).
- [12] R. A. Duine, K.-J. Lee, S. S. P. Parkin, and M. D. Stiles, Synthetic antiferromagnetic spintronics, *Nat. Phys.* **14**, 217 (2018).
- [13] R. Lebrun, A. Ross, S. A. Bender, A. Qaiumzadeh, L. Baldrati, J. Cramer, A. Brataas, R. A. Duine, and M. Kläui, Tunable long-distance spin transport in a crystalline antiferromagnetic iron oxide, *Nature* **561**, 222 (2018).
- [14] M. Althammer, Pure spin currents in magnetically ordered insulator/normal metal heterostructures, *J. Phys. D: Appl. Phys.* **51**, 313001 (2018).
- [15] K. Ando, S. Takahashi, K. Harii, K. Sasage, J. Ieda, S. Maekawa, and E. Saitoh, Electric Manipulation of Spin Relaxation Using the Spin Hall Effect, *Phys. Rev. Lett.* **101**, 036601 (2008).
- [16] I. M. Miron, K. Garello, G. Gaudin, P.-J. Zermatten, M. V. Costache, S. Auffret, S. Bandiera, B. Rodmacq, A. Schuhl, and P. Gambardella, Perpendicular switching of a single ferromagnetic layer induced by in-plane current injection, *Nature* **476**, 189 (2011).
- [17] X. Jia, K. Liu, K. Xia, and G. E. W. Bauer, Spin transfer torque on magnetic insulators, *EPL (Europhys. Lett.)* **96**, 17005 (2011).
- [18] L. Liu, C.-F. Pai, Y. Li, H. W. Tseng, D. C. Ralph, and R. A. Buhrman, Spin-torque switching with the giant spin Hall effect of tantalum, *Science* **336**, 555 (2012).
- [19] H. Nakayama, M. Althammer, Y.-T. Chen, K. Uchida, Y. Kajiwara, D. Kikuchi, T. Ohtani, S. Geprägs, M. Opel, S. Takahashi, R. Gross, G. E. W. Bauer, S. T. B. Goennenwein, and E. Saitoh, Spin Hall Magnetoresistance Induced by a Nonequilibrium Proximity Effect, *Phys. Rev. Lett.* **110**, 206601 (2013).
- [20] N. Vlietstra, J. Shan, V. Castel, B. J. van Wees, and J. Ben Youssef, Spin-Hall magnetoresistance in platinum on yttrium iron garnet: Dependence on platinum thickness and in-plane/out-of-plane magnetization, *Phys. Rev. B* **87**, 184421 (2013).
- [21] M. Althammer *et al.*, Quantitative study of the spin Hall magnetoresistance in ferromagnetic insulator/normal metal hybrids, *Phys. Rev. B* **87**, 224401 (2013).
- [22] Y.-T. Chen, S. Takahashi, H. Nakayama, M. Althammer, S. T. B. Goennenwein, E. Saitoh, and G. E. W. Bauer, Theory of spin Hall magnetoresistance, *Phys. Rev. B* **87**, 144411 (2013).
- [23] A. Kobs, S. Heße, W. Kreuzpaintner, G. Winkler, D. Lott, P. Weinberger, A. Schreyer, and H. P. Oepen, Anisotropic Interface Magnetoresistance in Pt/Co/Pt Sandwiches, *Phys. Rev. Lett.* **106**, 217207 (2011).
- [24] M. Coll *et al.*, Towards oxide electronics: A roadmap, *Appl. Surf. Sci.* **482**, 1 (2019).
- [25] K. Ganzhorn, J. Barker, R. Schlitz, B. A. Piot, K. Ollefs, F. Guillou, F. Wilhelm, A. Rogalev, M. Opel, M. Althammer, S. Geprägs, H. Huebl, R. Gross, G. E. W. Bauer, and S. T. B. Goennenwein, Spin Hall magnetoresistance in a canted ferrimagnet, *Phys. Rev. B* **94**, 094401 (2016).
- [26] G. R. Hoogeboom, A. Aqeel, T. Kuschel, T. T. M. Palstra, and B. J. van Wees, Negative spin Hall magnetoresistance of Pt on the bulk easy-plane antiferromagnet NiO, *Appl. Phys. Lett.* **111**, 052409 (2017).
- [27] J. Fischer, O. Gomonay, R. Schlitz, K. Ganzhorn, N. Vlietstra, M. Althammer, H. Huebl, M. Opel, R. Gross, S. T. B. Goennenwein, and S. Geprägs, Spin Hall magnetoresistance in antiferromagnet/heavy-metal heterostructures, *Phys. Rev. B* **97**, 014417 (2018).
- [28] L. Baldrati, A. Ross, T. Niizeki, C. Schneider, R. Ramos, J. Cramer, O. Gomonay, M. Filianina, T. Savchenko, D. Heinze, A. Kleibert, E. Saitoh, J. Sinova, and M. Kläui, Full angular dependence of the spin Hall and ordinary magnetoresistance in epitaxial antiferromagnetic NiO(001)/Pt thin films, *Phys. Rev. B* **98**, 024422 (2018).
- [29] Y. Ji, J. Miao, Y. M. Zhu, K. K. Meng, X. G. Xu, J. K. Chen, Y. Wu, and Y. Jiang, Negative spin Hall magnetoresistance in antiferromagnetic Cr<sub>2</sub>O<sub>3</sub>/Ta bilayer at low temperature region, *Appl. Phys. Lett.* **112**, 232404 (2018).
- [30] S. DuttaGupta, R. Itoh, S. Fukami, and H. Ohno, Angle dependent magnetoresistance in heterostructures with antiferromagnetic and non-magnetic metals, *Appl. Phys. Lett.* **113**, 202404 (2018).
- [31] S. Meyer, M. Althammer, S. Geprägs, M. Opel, R. Gross, and S. T. B. Goennenwein, Temperature dependent spin transport properties of platinum inferred from spin Hall magnetoresistance measurements, *Appl. Phys. Lett.* **104**, 242411 (2014).
- [32] M. Althammer, A. V. Singh, T. Wimmer, Z. Galazka, H. Huebl, M. Opel, R. Gross, and A. Gupta, Role of interface quality for the spin Hall magnetoresistance in nickel ferrite thin films with bulk-like magnetic properties, *Appl. Phys. Lett.* **115**, 092403 (2019).
- [33] R. Schlitz, T. Kosub, A. Thomas, S. Fabretti, K. Nielsch, D. Makarov, and S. T. B. Goennenwein, Evolution of the spin Hall magnetoresistance in Cr<sub>2</sub>O<sub>3</sub>/Pt bilayers close to the Néel temperature, *Appl. Phys. Lett.* **112**, 132401 (2018).

- [34] S. Vélez, V. N. Golovach, J. M. Gomez-Perez, A. Chuvalin, C. T. Bui, F. Rivadulla, L. E. Hueso, F. S. Bergeret, and F. Casanova, Spin Hall magnetoresistance in a low-dimensional Heisenberg ferromagnet, *Phys. Rev. B* **100**, 180401(R) (2019).
- [35] P. Villars, PAULING FILE, in Inorganic Solid Phases, SpringerMaterials (online database), Springer, Heidelberg (ed.), SpringerMaterials,  $\alpha$ -Fe<sub>2</sub>O<sub>3</sub>, hematite (Fe<sub>2</sub>O<sub>3</sub> hem) Crystal Structure. [https://materials.springer.com/isp/crystallographic/docs/sd\\_1605430](https://materials.springer.com/isp/crystallographic/docs/sd_1605430).
- [36] F. J. Morin, Magnetic susceptibility of  $\alpha$ Fe<sub>2</sub>O<sub>3</sub> and  $\alpha$ Fe<sub>2</sub>O<sub>3</sub> with added titanium, *Phys. Rev.* **78**, 819 (1950).
- [37] C. G. Shull, W. A. Strauser, and E. O. Wollan, Neutron diffraction by paramagnetic and antiferromagnetic substances, *Phys. Rev.* **83**, 333 (1951).
- [38] I. Dzyaloshinsky, A thermodynamic theory of “weak” ferromagnetism of antiferromagnetics, *J. Phys. Chem. Solids* **4**, 241 (1958).
- [39] T. Moriya, Anisotropic superexchange interaction and weak ferromagnetism, *Phys. Rev.* **120**, 91 (1960).
- [40] A. H. Morrish, *Canted Antiferromagnetism: Hematite* (World Scientific, Singapore, 1994).
- [41] R. Nathans, S. J. Pickart, H. A. Alperin, and P. J. Brown, Polarized-neutron study of hematite, *Phys. Rev.* **136**, A1641 (1964).
- [42] J. C. Marmeggi, D. Hohlwein, and E. F. Bertaut, Magnetic neutron Laue diffraction study of the domain distribution in  $\alpha$ -Fe<sub>2</sub>O<sub>3</sub>, *Phys. Status Solidi (a)* **39**, 57 (1977).
- [43] M. Opel, S. Geprägs, M. Althammer, T. Brenninger, and R. Gross, Laser molecular beam epitaxy of ZnO thin films and heterostructures, *J. Phys. D: Appl. Phys.* **47**, 034002 (2014).
- [44] See the Supplemental Material at <http://link.aps.org/supplemental/10.1103/PhysRevApplied.13.014019> for the extended structural characterization (x-ray reflectivity, atomic force microscopy), the magnetic characterization (hysteresis curve) via superconducting-quantum-interference-device (SQUID) magnetometry, the mathematical description of the SMR oscillations, and additional SMR data.
- [45] G. S. Parkinson, Iron oxide surfaces, *Surf. Sci. Rep.* **71**, 272 (2016).
- [46] X.-G. Wang, W. Weiss, S. K. Shaikhutdinov, M. Ritter, M. Petersen, F. Wagner, R. Schlögl, and M. Scheffler, The Hematite ( $\alpha$ -Fe<sub>2</sub>O<sub>3</sub>) (0001) Surface: Evidence for Domains of Distinct Chemistry, *Phys. Rev. Lett.* **81**, 1038 (1998).
- [47] B.-W. Dong, L. Baldrati, C. Schneider, T. Niizeki, R. Ramos, A. Ross, J. Cramer, E. Saitoh, and M. Kläui, Antiferromagnetic NiO thickness dependent sign of the spin Hall magnetoresistance in  $\gamma$ -Fe<sub>2</sub>O<sub>3</sub>/NiO/Pt epitaxial stacks, *Appl. Phys. Lett.* **114**, 102405 (2019).
- [48] L. Zhu, D. C. Ralph, and R. A. Buhrman, Effective Spin-Mixing Conductance of Heavy-Metal–Ferromagnet Interfaces, *Phys. Rev. Lett.* **123**, 057203 (2019).
- [49] Y. Yang, Y. Xu, K. Yao, and Y. Wu, Thickness dependence of spin Hall magnetoresistance in FeMn/Pt bilayers, *AIP Adv.* **6**, 065203 (2016).
- [50] F. D. Czeschka, L. Dreher, M. S. Brandt, M. Weiler, M. Althammer, I.-M. Imort, G. Reiss, A. Thomas, W. Schoch, W. Limmer, H. Huebl, R. Gross, and S. T. B. Goennenwein, Scaling Behavior of the Spin Pumping Effect in Ferromagnet–Platinum Bilayers, *Phys. Rev. Lett.* **107**, 046601 (2011).
- [51] Y. Cheng, S. Yu, A. S. Ahmed, M. Zhu, J. Hwang, and F. Yang, Anisotropic magnetoresistance and nontrivial spin magnetoresistance in Pt/ $\alpha$ -Fe<sub>2</sub>O<sub>3</sub> bilayers: Evidence for antiferromagnetic proximity effect, *Phys. Rev. B* **100**, 220408 (2019).
- [52] T. Shang, Q. F. Zhan, H. L. Yang, Z. H. Zuo, Y. L. Xie, L. P. Liu, S. L. Zhang, Y. Zhang, H. H. Li, B. M. Wang, Y. H. Wu, S. Zhang, and R.-W. Li, Effect of NiO inserted layer on spin-Hall magnetoresistance in Pt/NiO/YIG heterostructures, *Appl. Phys. Lett.* **109**, 032410 (2016).
- [53] D. Hou, Z. Qiu, J. Barker, K. Sato, K. Yamamoto, S. Vélez, J. M. Gomez-Perez, L. E. Hueso, F. Casanova, and E. Saitoh, Tunable Sign Change of Spin Hall Magnetoresistance in Pt/NiO/YIG Structures, *Phys. Rev. Lett.* **118**, 147202 (2017).
- [54] W. Lin and C. L. Chien, Electrical Detection of Spin Backflow from an Antiferromagnetic Insulator/Y<sub>3</sub>Fe<sub>5</sub>O<sub>12</sub> Interface, *Phys. Rev. Lett.* **118**, 067202 (2017).
- [55] Y.-M. Hung, C. Hahn, H. Chang, M. Wu, H. Ohldag, and A. D. Kent, Spin transport in antiferromagnetic NiO and magnetoresistance in Y<sub>3</sub>Fe<sub>5</sub>O<sub>12</sub>/NiO/Pt structures, *AIP Adv.* **7**, 055903 (2017).
- [56] J. A. Eaton and A. H. Morrish, Magnetic domains in hematite at and above the Morin transition, *J. Appl. Phys.* **40**, 3180 (1969).
- [57] G. F. Clark, P. A. Goddard, J. R. S. Nicholson, B. K. Tanner, and B. M. Wanklyn, Evidence for very-large-area magnetic domain walls in haematite ( $\alpha$ -Fe<sub>2</sub>O<sub>3</sub>), *Philos. Mag. B* **47**, 307 (1983).
- [58] A. Ross, R. Lebrun, O. Gomonay, D. A. Grave, A. Kay, L. Baldrati, S. Becker, A. Qaiumzadeh, C. Ulloa, G. Jakob, F. Kronast, J. Sinova, R. Duine, A. Brataas, A. Rothschild, and M. Kläui, Propagation length of antiferromagnetic magnons governed by domain configurations, *Nano Lett.* **20**, 306 (2020).
- [59] F. Bødker, M. F. Hansen, C. B. Koch, K. Lefmann, and S. Mørup, Magnetic properties of hematite nanoparticles, *Phys. Rev. B* **61**, 6826 (2000).
- [60] R. A. Voskanyan, R. Z. Levitin, and V. A. Shchurov, Magnetostriction of a hematite monocrystal in fields up to 150 kOe, Sov. Phys. JETP **27**, 423 (1968), <http://jetp.ac.ru/cgi-bin/e/index/e/27/3/p423?a=list>
- [61] T. Yamada, S. Saito, and Y. Shimomura, Magnetic anisotropy, magnetostriction, and magnetic domain walls in NiO. II. Experiment, *J. Phys. Soc. Jpn.* **21**, 672 (1966).